# Comparative Performance Assessment of Circular and Linear Polarized Antennas used for Doppler Radar Measurement of Respiratory Motion

Jon Itokazu
Dept. of Electrical and Computer
Engineering
University of Hawai'i at Mānoa
Honolulu, USA
jitokazu@hawaii.edu

Olga Boric-Lubecke
Dept. of Electrical and Computer
Engineering
University of Hawai'i at Mānoa
Honolulu, USA
olgabl@hawaii.edu

Marija Milijić
Faculty of Electrical Engineering
University of Niš
Niš, Serbia
marija.milijic@elfak.ni.ac.rs

Victor Lubecke
Dept. of Electrical and Computer
Engineering
University of Hawai'i at Mānoa
Honolulu, USA
lubecke@hawaii.edu

Branka Jokanović
Institute of Physics
University of Belgrade, and The
Academy of Engineering Sciences of
Serbia
Belgrade, Serbia
brankaj@ipb.ac.rs

Abstract— The quality of human respiratory motion measurements made with Doppler radar depends on the amount of reflected signal received and the overall signal to noise ratio (SNR) of the measurement. The non-uniform characteristics of the human torso and its motion impact both the amount of signal returned toward the radar and its polarization. This study used a 2.4 GHz continuous wave Doppler radar system to compare the respiratory motion measurement performance for circular polarized antennas and linear polarized antennas, using mechanical respiratory phantom measurements at a nominal distance of one meter. While the different surfaces examined produced varied levels of signal at the original and other polarizations, the measurements using circular polarized antennas consistently provided less overall received signal and no significant improvement of SNR.

Keywords— Physiological radar, circular polarized antenna, human respiration

# I. INTRODUCTION

In traditional radar applications, uneven surfaces generate variously polarized reflections, and polarimetric radar methods have been applied to study how to best capture and analyze return signatures [1]–[4]. A human study conducted in [5] concluded that the irregular surfaces of the human torso generate significant amounts of cross-polarization. So far, physiological Doppler radar research has been mainly restricted to linear polarizations. An approach using circularly polarized antennas was explored in [6] but was only for the purpose of better transmit/receive isolation and did not assess the radar's performance as a physiological radar [7]–[9].

This paper aims to comparatively assess the performance of circularly polarized antennas (CP) and linearly polarized (LP) antennas for physiological radar. Measurements were taken for three different mechanical respiratory phantoms at a nominal distance of one meter using a 2.4-GHz physiological Doppler radar system. The results using CP antennas and LP antennas were compared for both return signal strength and signal to noise

This work was supported in part by the National Science Foundation (NSF) under grants IIS 1915738, and CNS2039089, and by the Ministry of Science, Technological Development and Innovations of the Republic Serbia

ratio (SNR). Measurements made using LP antennas were found to consistently produce stronger return signals, while CP signals did not provide significant improvement in SNR. The experimental setup used to acquire the measurements is discussed in Section II, followed by an analysis and comparison of the performance metrics of linear and circular antenna configurations in Section III. In Section IV, the performance of LP antennas and CP antennas is assessed and discussed.

## II. EXPERIMENTAL SETUP

# A. Mover and Phantom Torso Setup

For this assessment, three phantom torsos, shown in Figure 1(a-c), were designed and constructed to approximate the characteristics of human breathing with a simple model capable of capturing salient information [5]. The flat rectangular plate (RP) had dimensions of 32 cm x 30 cm and the single half cylinder (SHC) and double half cylinder (DHC) shared the same dimensions of 32 cm x 30 cm, but with different radii—15 cm for the SHC and 7.5 cm for the DHC.

Each robotic phantom was mounted onto a single-axis precision linear motion platform (Griffin Motion). The motion platform was controlled by a Galil DMC-30012 motion controller and positioned at a nominal distance of 1m away from the Tx/Rx antennas to minimize the effect of slight deviations in antenna placement and alignment. Each robotic phantom was programmed to mimic a 4.0-cm displacement, at a rate of 0.2 Hz (12 breaths per minute).

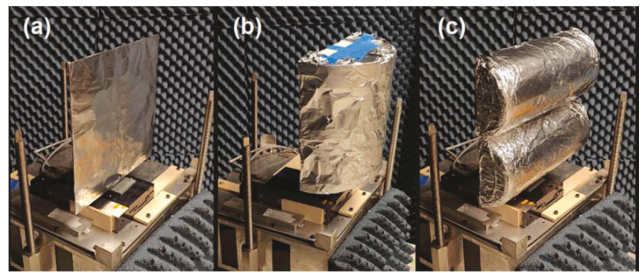


Figure 1: Phantom torsos mounted onto a motion platform (a) flat rectangular plate (RP) (b) single half cylinder (SHC), and (c) double half cylinder (DHC)

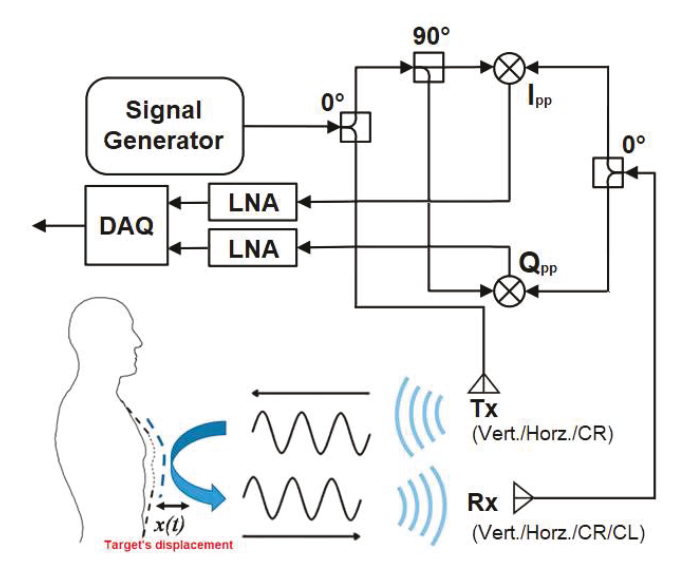


Figure 2: Schematic of Radar System and Antenna Configurations

# B. Radar Setup

The radar system used to obtain the data consisted of a signal generator (HP E4433B), set to deliver a 2.4 GHz, +10 dBm input signal; two 0°-splitters (ZFSC-2-2500-S+); two mixers (ZFM-4212+); and a single 90°-splitter (ZX10Q-2-25-S+). Six antenna arrangements were used; four used LP antennas (L-COM RE09P-SM), and two used right handed (CR) circularly polarized (L-COM HG2409PCR-SM) and left handed (CL) circularly polarized antennas (L-COM HG2409PCL-SM).

For the LP antennas, each transmit configuration was measured with both vertical and horizontal receive antenna configurations. The CP antennas were arranged with CR polarized transmit and measured with both CL and CR polarized

receive antennas. For every phantom, a laser measure (Bosch GLM100-23) was used to align the target with the antennas and multiple datasets were obtained for each measurement to ensure antenna placement was not significantly impacting the results.

The I- and Q-channel outputs are extracted from each channel's mixer, then amplified and filtered using two LNAs (SR560). Both LNAs were configured with a gain of 20 and filtered using the on-board low-pass filter settings with a cutoff of 10 Hz and a 6 dB/dec roll-off. The outputs of the LNAs were routed through a terminal block (NI BNC-2111) and DAQ (NI USB-6281), and then sent to a readout PC.

# III. ANALYSIS AND COMPARISON

The I- and Q-channel peak-to-peak data was filtered in MATLAB using the "lowpass" function provided in the signal processing toolbox. Applying the techniques described in [10], amplitude and phase imbalance coefficients were calculated and applied to correct the LP and CP datasets. With exception of the RP phantom, the CP datasets were obtained with both, vertically and horizontally oriented phantoms to assess the CP antennas' sensitivity to target orientation.

The amplitude and phase corrected datasets were then ellipse-fit using the Levenberg-Marquartdt algorithm [11] to obtain the estimated center of each dataset and its respective estimated radius,  $r_{\rm fit}$ . The estimated centers were then used to perform offset correction and center each dataset at the origin of the I/Q-plane. The datasets were then arctangent demodulated to obtain the displacement information. In this section, the I/Q data, radius deviation, and demodulated data obtained using LP and CP antennas are compared for each phantom torso and tabulated in Table 1.

# A. Comparison of I vs. Q.

A visual comparison of the I/Q data obtained using LP and CP antennas for the DHC target is depicted in Figure 3. The

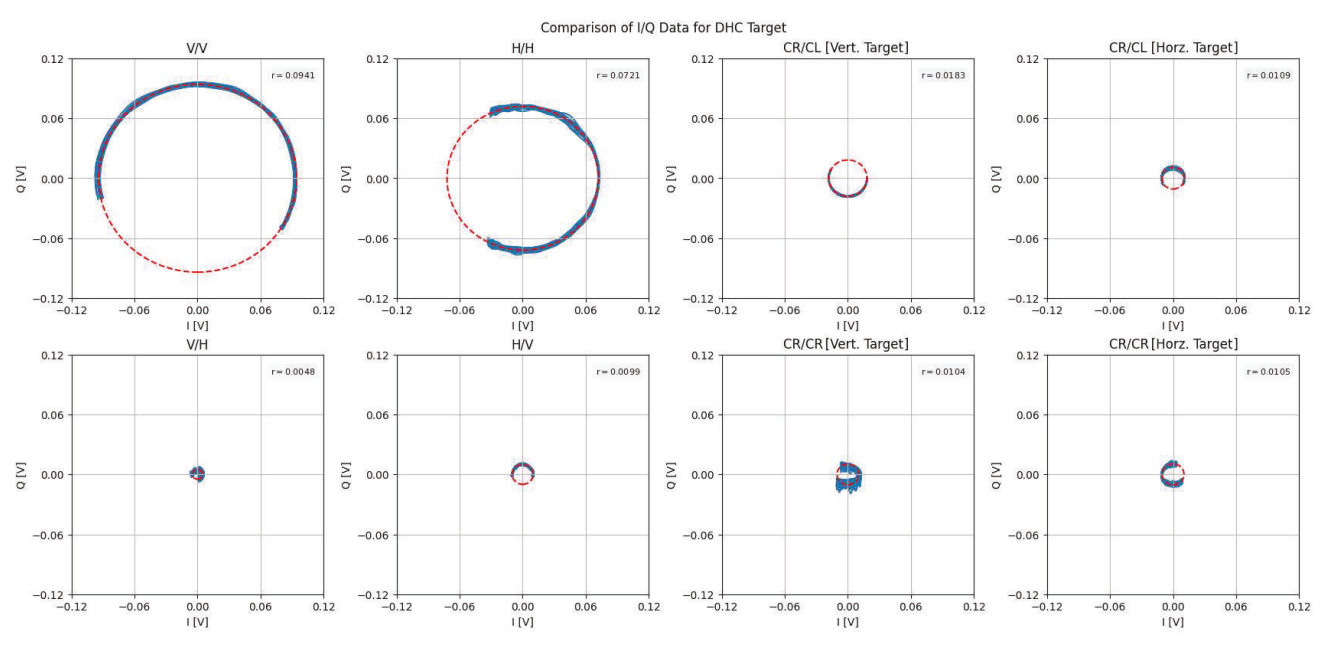


Figure 3: Representative plots of the amplitude, phase, and offset corrected I/Q data showing a comparison of the reflected power for a single phantom (DHC). The radii of the co-polarized measurements made using LP antennas (V/V and H/H) are almost a whole order of magnitude larger than all other measurements made. Comparison of the thickness of the arctangent demodulated trace (blue) shows no significant improvement in of SNR.

TABLE I
PERFORMANCE METRICS OF LINEAR AND CIRCULAR ANTENNA CONFIGURATIONS

Antenna Polarization		RP			SHC			DHC		
Tx/Rx		r [mV]	SNR <sup>a</sup> [%]	Error Rate <sup>b</sup> [%]	r [mV]	SNR <sup>a</sup> [%]	Error Rate <sup>b</sup> [%]	r [mV]	SNR <sup>a</sup> [%]	Error Rate <sup>b</sup> [%]
V/V		197.01	0.38	4.95	86.83	1.32	0.95	94.11	1.01	2.52
V/H		3.77	30.99	73.90	6.12	19.56	11.23	4.83	24.79	28.08
H/V		12.71	5.84	21.98	2.46	1.50	50.67	9.92	5.73	9.78
H/H		210.87	0.31	8.29	61.95	11.88	1.25	72.05	2.10	2.06
Vert.Oriented Target	CR/CL	24.29	6.30	9.95	12.12	2.04	0.40	18.26	1.59	7.45
	CR/CR	23.42	7.15	9.80	7.33	24.14	28.06	10.36	22.78	33.80
Horz.Oriented Target	CR/CL	2	-	-	9.43	2.62	5.60	10.85	4.37	6.06
	CR/CR	-	-	-	9.76	4.20	8.38	10.48	11.52	10.84

<sup>&</sup>lt;sup>a</sup> The effective SNR, defined in (3), was scaled by a factor of 100 and radii deviations are reported in percent of the ellipse-fit radii

arctangent demodulated radius, which is a measure of the reflected power, is defined as

$$\left| \widetilde{r(t)} \right| = \sqrt{V_I^2(t) + V_Q^2(t)} \tag{1}$$

and is plotted in blue. The estimated radius,  $r_{\rm fit}$ , is depicted in the plots by the dashed red traces and represents the values reported in Table 1. Figure 3 and Table 1 clearly show the measurements using CP antennas consistently provided less overall received signal. In particular, measurements made with the co-polarized linear antennas (V/V and H/H) were, on average, between 5.7 and 8.4 times greater than measurements made with their circular counterparts (CR/CL Vert. and Horz. oriented targets). The lower received signal power when using CP antennas is likely due to scattering from non-ideal surfaces leaving only small portion of the signal reflected in CL polarization.

Although there were slight variations between phantoms, for any given phantom, e.g., SHC or DHC, the values of estimated radii when the target was vertically oriented (V/V and CR/CL Vert.) were 1.3–1.7 times larger than when the target was horizontally oriented (H/H and CR/CL Horz.).

In general, the linearly co-polarized (V/V and H/H) and circularly cross-polarized (CR/CL) transmit and receive configurations have better performance metrics (e.g., larger radius, lower effective SNR, and/or lower error rates) than their counterparts, i.e., V/H and H/V for LP and CR/CR for CP antennas. As such, the authors will refer to the former and latter as "dominant" and "non-dominant" polarization configurations, respectively, for the remainder of this work.

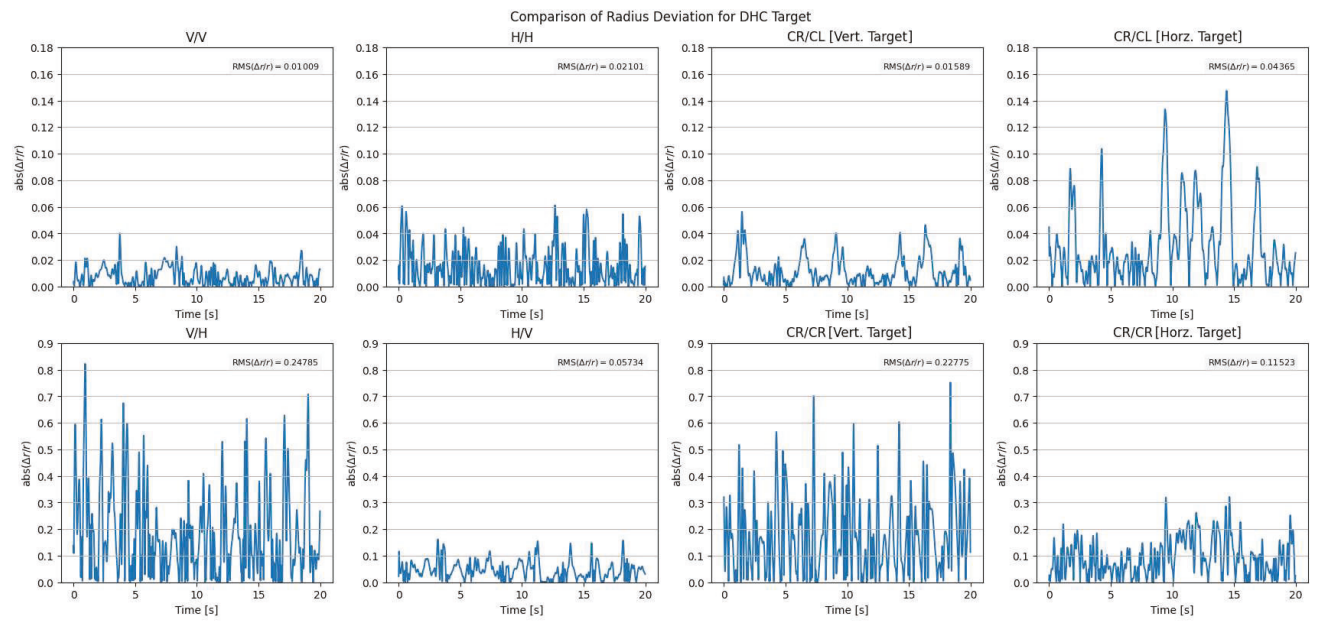


Figure 4: Representative plots of the effective SNR showing a comparison of how much the arctangent demodulated radius deviates from the fit radius. An value of 1.0 indicates deviations equal to the magnitude of the fit radius.

b Error rate = |Measured Displacement - Nominal Displacement|/Nominal Displacement, where the nominal displacement is 4.0 cm.

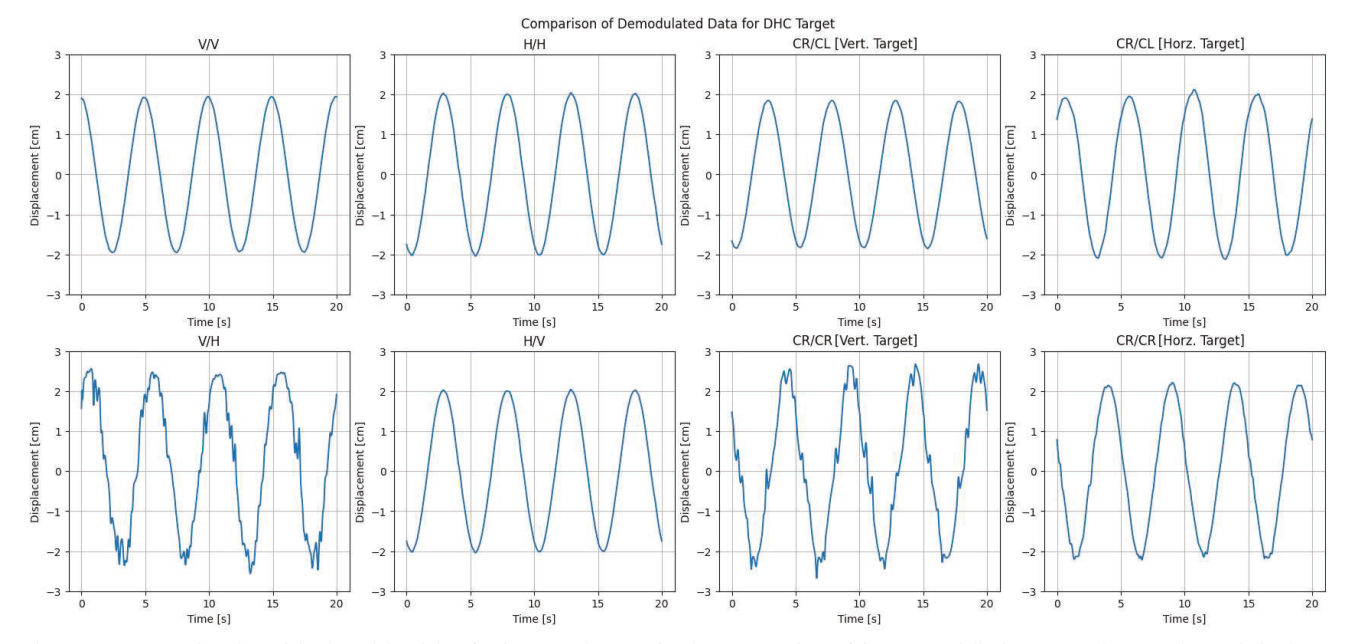


Figure 5: Representative plots of the demodulated data for the DHC phantom showing a comparison of the measured displacements taken at various polarizations.

# B. Comparison of Radius Deviation

The thickness of the blue I/Q traces shown in the plots of Figure 3 serves as a visual representation of the extent of the effective noise for a particular signal measurement. The thicker the trace, the further the demodulated radius  $|\widetilde{r(t)}|$  deviates from the estimated radius  $r_{\rm fit}$ . These deviations about the estimated radius (dashed red), are given by

$$\Delta r = \left| \widetilde{r(t)} \right| - r_{\text{fit}}. \tag{2}$$

Equation (2) represents small changes in the demodulated radius and is used to quantify the SNR. For a comparison independent of amount of received power, (2) is normalized to  $r_{\rm fit}$  and the absolute value is taken to quantify deviations without regard to direction (increases or decreases about  $r_{\rm fit}$ ), resulting in

SNR = 
$$abs(\Delta r/r_{fit})$$
, (3)

which is used to effectively quantify the SNR for each configuration. Noting that this "effective" SNR (3) is a function of time, the RMS of these normalized deviations were calculated, scaled by a factor of 100, and reported in percent in Table 1 for all polarization configurations.

The effective SNR for dominant polarization configurations varied slightly between the three phantoms, but were all low in value and comparable with each other. The SNR for non-dominant configurations varied between the three phantoms and was consistently higher than that of the dominant configurations, indicating no differences or improvement of SNR between using LP and CP antennas.

Figure 4 shows a visual comparison of SNR for the DHC phantom and shows that the dominant polarization configurations have similar levels of SNR, while the non-dominant polarization configurations vary between high and low

amounts. This variation is the result of the amount of received signal and indicates a dependence on the orientation of the target.

# C. Comparison of Demodulated Data

Representative plots of the demodulated data for the DHC phantom are shown in Figure 5 which compares the displacement waveforms acquired by each antenna configuration. Noting a nominal maximum displacement of 4.0 cm, the absolute displacement was obtained from these waveforms and used to calculate the error rates shown in Table 1

Between all three phantoms, the RP phantom exhibited the some of the highest error rates. The high error rates for the cross-polarized measurements are due to the reflected signals having very low power. The error rates of the co-polarized measurements for the RP phantom are due to edge effects and alignment sensitivity.

While the performance varied between phantoms, the dominant LP configurations consistently had similar or slightly lower error rates than the dominant CP configurations. The error rates of the non-dominant configurations were consistently higher than that of the dominant configurations and varied between phantoms.

# IV. CONCLUSION

While the different surfaces examined in this work produced varied levels of signal at the original and other polarizations, when compared with LP antennas, the measurements using CP antennas consistently provided less overall received signal and no significant improvement of SNR.

Additionally, all of the antenna configurations exhibited sensitivity to target orientation. In general, the performance of dominant configurations are only slightly changed when the target is rotated 90°. For LP antennas, this is apparent by comparing the V/V and H/H polarizations for each phantom. The performance of the non-dominant configurations are much more

sensitive to orientation changes in the target, and typically will have better performance metrics in one orientation as opposed to the other (e.g., V/H vs H/V, or Vert. CR/Horz. CR).

As a result, if the target being measured is oriented suboptimally, a radar system utilizing CP antennas, in any configuration, would not be able to recover that information unless the target changed to a more favorable orientation. An advantage LP antennas have over CP is that they can be used to configure a fully polarimetric radar system which can recover that same information without having to physically rotate the target.

### REFERENCES

- [1] J. D. Díaz Díaz, D. Schvartzman, J. L. Salazar-Cerreño, T.-Y. Yu, R. D. Palmer and M. S. McCord, "Polarimetric Atmospheric Imaging Radar (PAIR): Antenna Design, Testing, and Validation," 2022 IEEE Radar Conf. (RadarConf22), New York City, NY, USA, 2022, pp. 1-5.
- [2] B. Walther, A. Froehly, R. Herschel, M. van Delden, P. Wallrath and T. Musch, "A Fully Polarimetric Radar System for Non-Destructive Testing of Fiber Glass Layers," in *IEEE Trans. on Radar Syst.*, vol. 1, pp. 264-278, 2023.
- [3] S. Zhou, X. Zhang, H. Liu and Y. Zhao, "Polarimetric MIMO radar target detection," 2016 CIE International Conf. on Radar (RADAR), Guangzhou, China, 2016, pp. 1-4.
- [4] R. D. Palmer et al., "Horus—A Fully Digital Polarimetric Phased Array Radar for Next-Generation Weather Observations," in *IEEE Transactions* on Radar Systems, vol. 1, pp. 96-117, 2023.
- [5] J. Itokazu, M. Milijić, B. Jokanović, O. Boric-Lubecke, and V. Lubecke, "Analysis of Polarimetric Radar Effects in Respiratory Measurements," 2024 IEEE MTT-S Int. Microw. Biomed. Conf. (IMBioC), Montreal, Canada, Jun. 2024, [accepted].
- [6] Y. He, C. Gu, H. Ma, J. Zhu and G. V. Eleftheriades, "Miniaturized Circularly Polarized Doppler Radar for Human Vital Sign Detection," in *IEEE Trans. on Antennas and Propag.*, vol. 67, no. 11, pp. 7022-7030, Nov. 2019.
- [7] C. Gu et al., "Accurate Respiration Measurement Using DC-Coupled Continuous-Wave Radar Sensor for Motion-Adaptive Cancer Radiotherapy," in *IEEE Transactions on Biomed. Eng.*, vol. 59, no. 11, pp. 3117-3123, Nov. 2012.
- [8] A. Santra et al., "Short-Range Multi-Mode Continuous-Wave Radar for Vital Sign Measurement and Imaging," 2018 IEEE Radar Conf. (RadarConf18), Oklahoma City, OK, USA, 2018, pp. 946-950.
- [9] A. Santra et al., "Short-Range Multi-Mode Continuous-Wave Radar for Vital Sign Measurement and Imaging," 2018 IEEE Radar Conf. (RadarConf18), Oklahoma City, OK, USA, 2018, pp. 946-950.
- [10] M. Zakrzewski et al., "Quadrature Imbalance Compensation With Ellipse-Fitting Methods for Microwave Radar Physiological Sensing," in *IEEE Trans. on Microw. Theory and Techn.*, vol. 62, no. 6, pp. 1400-1408, June 2014.
- [11] X. Gao and O. Boric-Lubecke, "Radius Correction Technique for Doppler Radar Noncontact Periodic Displacement Measurement," in IEEE Trans. on Microw. Theory and Techn., vol. 65, no. 2, pp. 621-631, Feb. 2017